THE JOURNAL OF PHYSICAL CHEMISTRY B

Article

pubs.acs.org/JPCB

Thermodynamics and Kinetics of Gas Storage in Porous Liquids

Fei Zhang,[†] Fengchang Yang,[†] Jingsong Huang,[‡] Bobby G. Sumpter,[‡] and Rui Qiao*[,†]

[†]Department of Mechanical Engineering, Virginia Tech, Blacksburg, Virginia 24061, United States

[‡]Center for Nanophase Materials Sciences and Computer Science & Mathematics Division, Oak Ridge National Laboratory, Bethel Valley Road, Oak Ridge, Tennessee 37831, United States

Supporting Information

ABSTRACT: The recent synthesis of organic molecular liquids with permanent porosity opens up exciting new avenues for gas capture, storage, and separation. Using molecular simulations, we study the thermodynamics and kinetics for the storage of CH_4, CO_2, and N_2 molecules in porous liquids consisting of crown-ether-substituted cage molecules in a 15-crown-5 solvent. It is found that the intrinsic gas storage capacity per cage molecule follows the order $CH_4 > CO_2 > N_2$, which does not correlate simply with the size of gas molecules. Different gas molecules are stored inside the cage differently; e.g., CO_2 molecules prefer the cage's core whereas CH_4 molecules favor both the core and the branch regions. All gas molecules considered can enter the cage essentially without energy barriers and leave the cage on a nanosecond time scale by overcoming a modest energy penalty. The molecular mechanisms of these observations are clarified.

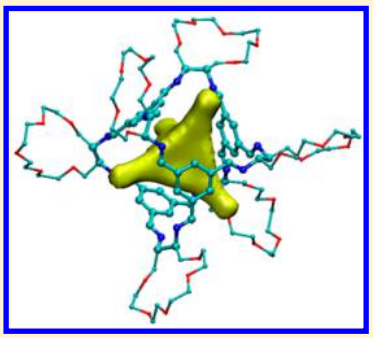

1. INTRODUCTION

Porous materials are indispensable in numerous applications such as molecular separation, energy storage, and catalysis.[1−3] However, most porous materials with permanent porosity, e.g., zeolites[4] and metal−organic frameworks (MOFs),[5] exist as solids. The solid nature of these materials poses certain degrees of restrictions on their processing, transport, and integration into engineering systems, especially at large scales. In comparison, porous liquids can potentially circumvent many of these restrictions because they are relatively easy to transport and process. There has been a long-standing interest in developing liquids with permanent, nanoscale porosity, and related research has led to many breakthroughs in recent years.[6−10] For example, the synthesis of rigid organic cage molecules[6] was considered to have initiated "a new branch in the evolutionary tree of porous materials" that is beyond zeolites and MOFs.[11] The intensive research on developing porous liquids culminated in the synthesis of the first liquids with permanent porosity in 2015.[12] Specifically, crown-ether functionalized diamines are coupled with 1,3,5-triformylbezenes, giving hollow organic cage molecules. The resulting molecules (i.e., the porosity units) were dissolved at high concentration into a 15-crown-5 solvent to produce porous liquids. Such liquids contain permanent cavities because neither the crown-ether side groups nor the solvent molecules can enter the organic cage molecule due to steric restrictions. It was demonstrated that the permanent cavities in these liquids afford an 8-fold increase of the solubility of methane molecules compared to that of the neat solvent.

The successful synthesis of permanently porous liquids opens up exciting new avenues for gas capture, storage, and separation. Nevertheless, there remains significant room to improve the performance of porous liquids; e.g., it is desirable to develop new porous liquids with improved gas storage capacity and superior selectivity toward different gas molecules. To help rationally design these materials, it is crucial to understand the molecular mechanisms of gas storage in porous liquids. Previous studies have provided valuable insights into some of these issues, e.g., using molecular dynamics (MD) simulations, the distribution of nanoscale cavities in the porous liquids has been clarified.[12] However, many important issues, in particular, the fundamental thermodynamics and kinetics of gas storage in the porous organic cage molecules, remain to be clarified. In this work, we studied the storage of different gas molecules including CH_4, CO_2, and N_2 in porous liquids made of crown-ether-substituted cage molecules dissolved in a 15-crown-5 solvent. Using MD simulations, we investigated the capacity and kinetics of the gas storage in the molecular cages. To elucidate the physics behind these macroscale characteristics, we also examined how gas molecules are stored inside the cage, the free energy landscape for gas molecules entering and leaving the cage, and the dynamic exchange between gas molecules inside and outside the cage.

2. SIMULATION SYSTEM AND METHODS

Figure 1a shows the molecular structure of the crown-ether-substituted cage, and Figure 1b highlights the functional motif of the cage for gas storage. Briefly, the cage has approximately an octahedral structure (marked with black lines in Figure 1b), which consists of a nonspherical cavity and four access windows (one of them is marked by a shaded triangle in Figure 1b) that allow gas molecules to enter/leave the cage. To facilitate discussions later, we define the entrance vectors of a cage as the

Received: May 11, 2016
Revised: June 30, 2016
Published: July 5, 2016

DOI: 10.1021/acs.jpcb.6b04784
J. Phys. Chem. B 2016, 120, 7195−7200

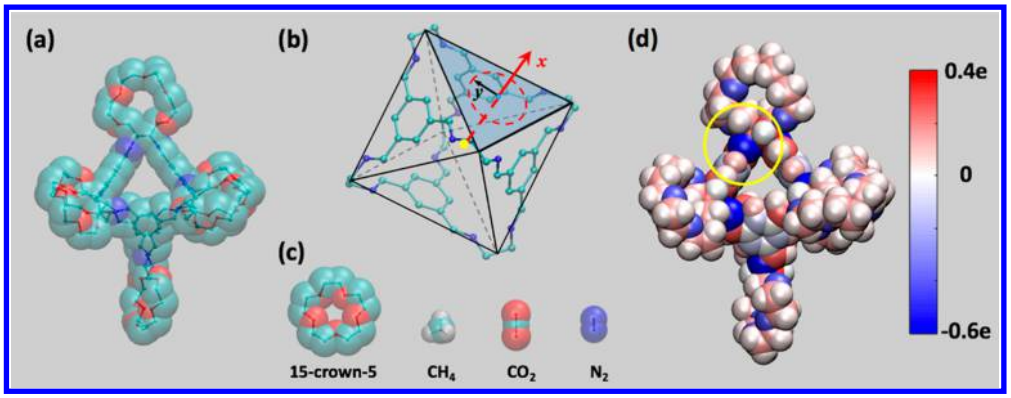

Figure 1. (a) Molecular structure of the cage molecule. (b) Schematic of the functional part of the cage molecule for gas storage. The yellow dot denotes the center of the cage cavity. The red arrow denotes the entrance vector of the cage molecule. (c) Molecular structure of the solvent molecule and the gas molecules. For clarity, hydrogen atoms of the cage molecule and the solvent molecule are not shown. (d) Partial atomic charge on the cage molecule (a list of the partial charge can be found in ref 12). The yellow circle highlights an imine atom with the largest partial charge, which is located near a vertex of the cage molecule.

vectors pointing from the center of the cage to the center of each of the four access windows (Figure 1b). Figure 1c shows the molecular structure of the solvent and the gas molecules studied. Figure 1d shows the partial atomic charges on the cage molecule as given by the force fields adopted here.

To study gas storage in the cage, we adopt a setup similar to the simulation system used by Giri et al.[12] Specifically, 20 cage molecules and 400 15-crown-5 solvents were mixed inside a periodic simulation box at a solvent−cage ratio of 20:1. Sixty gas molecules were dispersed into the cage−solvent mixture at a gas−cage ratio of 3:1, which creates an excess of gas molecules in the solvents. Compared to systems in which the porous liquids are in equilibrium with a gas reservoir, the present setup allows us to focus on studying the intrinsic gas storage capacity of molecular cages. The molecular structure of the solvent and three types of gases studied are shown in Figure 1c. The CH_4 molecule is roughly spherical with a diameter of ∼0.40 nm. The CO_2 molecule is rodlike, with a length and diameter of 0.53 and 0.34 nm, respectively. The N_2 molecule, also rodlike, is the smallest gas molecule considered here, with a length and diameter of 0.4 and 0.28 nm, respectively.

The OPLS-AA force fields[13] were used to describe the cage, solvent, and CH_4 molecules. CO_2 and N_2 molecules were modeled using the EPM2 and TraPPE force fields, respectively.[14,15] Of these force fields, those for CH_4, CO_2, and N_2 molecules are well established in prior studies of gas adsorption in MOFs.[16] The force fields for the cage molecules and the 15-crown-5 solvent are the same as those used in ref 12. To validate the force fields for the solvent, we simulated a pure 15-crown-5 solvent at 293.15 K and 1 atm. The solvent density was found to be 1.108 g/cm^3, in good agreement with the experimental value of 1.113 g/cm^3. In addition, simulations with the force fields used here for cage molecules reproduced the solubility of CH_4 gas in porous liquids.[12] Hence the force fields adopted in this study are adequate for the simulation of gas storage in porous liquids. We note that the flexibility of the cage molecules was taken into account in the force fields adopted here. However, simulations indicated that the cage molecule is rather rigid. Its shape fluctuation is minor when dispersed in the solvent (Figure S1 in the Supporting Information) and thus does not play a significant role in the gas storage.

MD simulations were performed in the isobaric−isothermal ensemble (T = 400 K and P = 1 atm) using the Gromacs code.[17] The PME method was used to calculate the electrostatic interactions with a real space cutoff of 1.4 nm and an FFT spacing of 0.12 nm. Nonelectrostatic interactions were computed with a cutoff length of 1.4 nm. Only the C−H bonds were constrained using the LINCS algorithm.[18] Simulations were performed using a time step of 1 fs, and the neighbor list was updated every step. To build the MD system, the cage and solvent molecules were first packed into the simulation box using the Packmol code.[19] The system was equilibrated for 5 ns before gas molecules were randomly inserted into the simulation box. An equilibrium run of 5 ns was then performed. To ensure that the system was sufficiently equilibrated, we examined the mean-square-displacement of the solvent and cage molecules, which diffuse much slower than the gas molecules and are thus more difficult to equilibrate. The results (Figure S2 in the Supporting Information) showed that, over a time period of 2 ns, a solvent molecule already diffuses ∼1 nm on average, which is larger than its size. Hence the solvent molecules are well equilibrated in the system. Over the same time period, a cage molecule diffused only several angstroms. However, because the cage−cage separation is large in our system (thus the gas storage depends mostly on the solvent and gas structure near the cage molecules), the limited center-of-mass movement of a cage molecule does not affect the evaluation of its gas storage capacity as long as solvents and gas in the system are sufficiently equilibrated. The equilibration run was followed by a 20 ns production run. For each gas studied, the simulation was repeated five times with different initial configurations to obtain reliable statistics.

3. RESULTS AND DISCUSSION

Capacity and Mode of Gas Storage. Figure 2 shows the accumulative count of gas molecules as a function of the distance from the center of the cage. Although the octahedral cage spans a maximum of ∼0.8 nm radially, the accumulative gas count increases very slowly at radial distances larger than ∼0.5 nm, indicating that few gas molecules are stored in this space. Examination of the structure of the cage (Figure 1b) shows that this space either is occupied by the cage atoms or is outside of the cage cavity. Hence, gas molecules located within a distance of 0.5 nm from the cage center are defined as being stored inside the cage. Using this definition and the data shown in Figure 2, the storage capacity of the cage was determined to

DOI: 10.1021/acs.jpcb.6b04784
J. Phys. Chem. B 2016, 120, 7195−7200

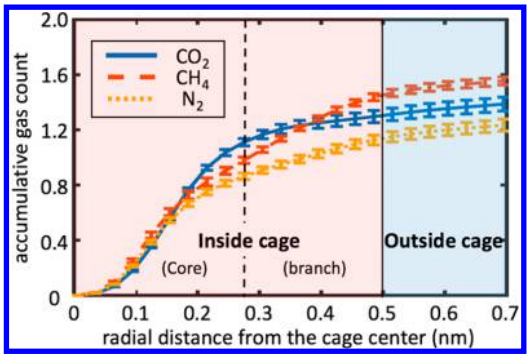

Figure 2. Accumulative gas molecule count as a function of the radial distance from the center of the cage. The position of a gas molecule is based on its center-of-mass.

be 1.47, 1.30, and 1.14 molecules for CH_4, CO_2, and N_2, respectively. These capacities are specific to the system studied here because they are affected by the overall density of the gas molecules in the *closed* MD system. Nevertheless, they provide an indication of the *relative* storage capability of the cage molecule for different gases and analysis of the gas distribution and energetics inside the cage molecule can provide insights into gas storage under practical conditions. Interestingly, the storage capacity does not correlate simply with the gas molecule's size: despite CH_4 being larger than the N_2 molecule, the cage hosts more CH_4 molecules than N_2 molecules. To understand the mechanism behind this peculiar observation and more generally the net storage capacity of the molecular cages, we further studied the molecular details of gas storage inside the cage.

Because the cavity inside a cage molecule is not spherical, how gas molecules are distributed inside a cage can greatly affect their storage. Hence, we examine the three-dimensional (3D) distribution of gas molecules inside the cage to delineate how they are stored. Figure 3 shows the isosurfaces of the

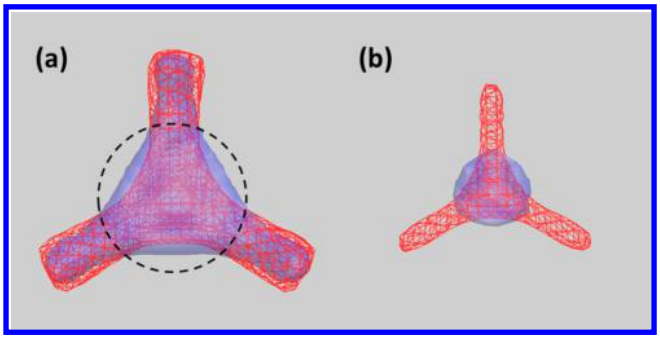

Figure 3. Isosurfaces of CO_2 (blue) and CH_4 (red) gas density inside the organic cage molecule. (a) Isosurfaces for a gas density of 2.8 nm^{-3}. (b) Isosurfaces for a gas density of 35 nm^{-3}. The black dashed line (radius: 0.28 nm) marks the boundary between the cage's core region and branch regions.

number density of CH_4 and CO_2 molecules inside the cage (the distributions of the N_2 molecules exhibit a behavior intermediate to that of the CH_4 and CO_2 molecules and are thus not shown). To illustrate which region within the cage the gas molecules can *access*, the isosurface is set to a number density of 2.8 nm^{-3} in Figure 3a, which is about 20 times of the gas density in bulk solvents but, nevertheless, small compared to the high gas density in some parts of the cage. Compared to the CH_4 molecules, CO_2 molecules access more (less) space in the central (peripheral) portion of the cage. To illustrate which region within the cage a given gas *prefers*, the isosurface is set to a number density of 35.0 nm^{-3} in Figure 3b. Figure 3b shows that CO_2 molecules favor the central part of the cage, whereas CH_4 molecules prefer the central and peripheral parts of the cage. These observations suggest partitioning the space inside the cage into two types of regions: (1) a "core" region at the center of the cage and (2) four rodlike "branch" regions close to the cage's four access windows (cf. Figure 1b). On the basis of the results in Figure 3, the boundary between these two types of regions can roughly be set at a distance of 0.28 nm from the cage's center (marked by the black dashed lines in Figures 2 and 3). With this partition, the storage capacity of a single cage for CH_4, CO_2, and N_2 molecules was found to be 1.0, 1.12, and 0.87 in its core region and 0.47, 0.18, and 0.27 in its branch regions.

The different storage capacities of the various gas molecules inside the cage's core region depend on the different gas−cage interactions. Specifically, the potential of a CO_2 molecule in the cage's core region due to its nonelectrostatic interactions (its attractive component represents the van der Waals interactions) with the cage was found to be −21.8 kJ/mol, which is stronger than that of a CH_4 molecule (−17.02 kJ/mol) and N_2 molecule (−12.95 kJ/mol). Therefore, gas molecules are energetically favored in the cage's core region in the order CO_2 > CH_4 > N_2. Because both CO_2 and N_2 molecules have notable quadrupole moments and charge−quadrupolar interactions play an important role in gas storage in porous materials such as zeolites,[20] we examine the distribution of the partial charges on the cage atoms and the electrostatic gas−cage interaction energy for the gas molecules in the cage's core region. We found that, although some atoms of the cage molecule carry notable charge (up to −0.6e, Figure 1d), the electrostatic gas−cage interactions are rather weak (−2.7 kJ/mol for the CO_2 molecules and −0.3 kJ/mol for the N_2 molecules) and thus play a very limited role in controlling gas storage in the cage. The weak electrostatic interactions are caused by two effects. First, gas molecules cannot approach closely the cage atoms carrying notable partial charges (mostly located near the vertices of the cage molecule, as highlighted by the yellow circle in Figure 1d) due to the obstruction by other atoms. Second, the electrostatic interactions between quadrupolar gas molecules CO_2 (or N_2) and charged cage atoms decay rapidly with charge−gas separation r (i.e., $\sim 1/r^3$).[20]

The storage capacities of different gases in the cage's branch region are affected by both the steric and the van der Waals interactions. For the CO_2 molecules, which are considerably longer than the N_2 molecules, because of their steric interactions with the cage atoms in the branch region, they mostly align with the cage's entrance vector upon entering the narrow branch regions (Figure 4). This restricts the CO_2 molecule's rotation and thus incurs an entropic penalty. Consequently, few CO_2 molecules are stored in the branch regions. For the nearly spherical CH_4 molecule, such an entropic penalty is minor. For the N_2 molecules, which are nearly randomly oriented with respect to the cage's entrance vector (Figure 4), such an entropic penalty is likewise minor. However, the CH_4 molecules interact with the cage atoms in the branch region through van der Waals forces more strongly than the N_2 molecules. This, along with the fact that the electrostatic interactions between the cage and gas molecules (N_2, CH_4, and CO_2) in the branch region are very weak, makes

DOI: 10.1021/acs.jpcb.6b04784
J. Phys. Chem. B 2016, 120, 7195−7200

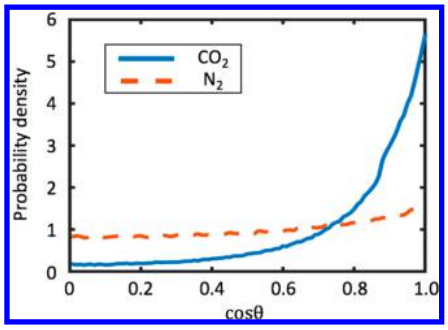

Figure 4. Distribution of the angle θ formed between a gas molecule's axis (O−C−O for CO_2 and N−N for N_2) and the cage molecule's entrance vector when the gas molecule resides in the branch region of the cage molecule.

the storage capacity of CH_4 molecules higher than that of the N_2 molecules in the branch regions.

Because gas molecules can distribute in different parts of a cage, it is possible that several gas molecules occupy the cage simultaneously. Figure 5 shows the probability distribution of

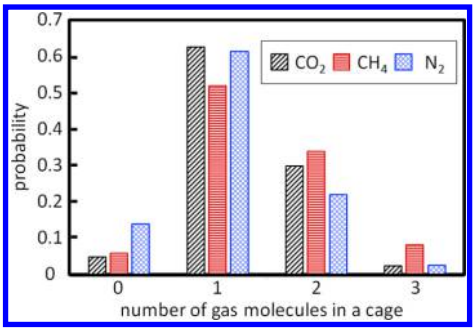

Figure 5. Probability distribution of the number of gas molecules inside a cage. The probability that four gas molecules occupy the same cage is <0.1% in the present system and is thus not shown.

the cage being occupied by different number of gas molecules. Overall, the probability of finding multiple molecules within a single cage is the highest for the CH_4 molecules. This can be attributed to the facts that (1) CH_4 molecules favor both the cage's core and branch regions and (2) CH_4 molecules are small enough that a cage can accommodate one CH_4 molecule in its core and a few more CH_4 molecules in its branch regions. For the CO_2 molecules, because they rarely reside in the cage's branch regions due to the large entropic penalty, storing two CO_2 molecules simultaneously inside the cage requires both molecules to be packed into the cage's core region, which is rather difficult. Consequently, finding multiple CO_2 molecules simultaneously inside one cage is more difficult than the case of CH_4 molecules. Although N_2 molecules are small enough for a cage to accommodate one N_2 molecule in its core and several other N_2 molecules in its branches, multiple occupancy is rare because they are attracted to the cage rather weakly. Also due to the weak interaction, N_2 has the highest probability of leaving a cage molecule.

On the basis of these results, we suggest that the storage of simple gas molecules in a given cage is controlled mainly by two factors: molecular gas−cage interactions that determine how strongly gas molecules are favored energetically inside the cage and the size/shape of the gas molecules that determine to what extent different storage spaces inside a given cage (i.e., the core and the branch regions) can be used *simultaneously*. The storage capacity is the highest for the CH_4 molecules because both factors are favorable for them. The storage capacity is lower for the CO_2 molecules because they cannot effectively make use of the cage's storage space in the narrow branch regions due to large entropic penalty. The storage capacity is the lowest for the N_2 molecules because their molecular interactions with the cage are weak, hence providing limited energetic benefit for N_2 molecules to be stored inside the cage.

Kinetics of Gas Storage. For practical application of porous liquids, one must understand not only the capacity of gas storage but also the kinetics of gas storage, i.e., how easy/difficult gas molecules enter/leave the cage. To answer this question, we calculated the potential of mean force (PMF) of gas molecules near and inside a cage molecule. Specifically, the PMF of gas molecules in and near the cage was computed using $\mathrm{PMF}(x,y) = k_B T \times \ln(\rho_n^{\infty}/\rho_n(x,y))$ where (x, y) is the position of the gas molecule with respect to the cage's entrance vector (see Figure 1b for definition), $k_B T$ is the thermal energy, ρ_n^{∞} is the number density of gas molecules in bulk solvents, and $\rho_n(x,y)$ is the gas density at a position (x, y). Note here the PMF in the bulk solvents is taken as zero. In the present system, the free energy landscape is relatively smooth (this is evident from the facile exchange between gas inside and outside the cage; see below). Hence, very good statistics of gas density and PMF can be obtained from long simulations without the need of steering.

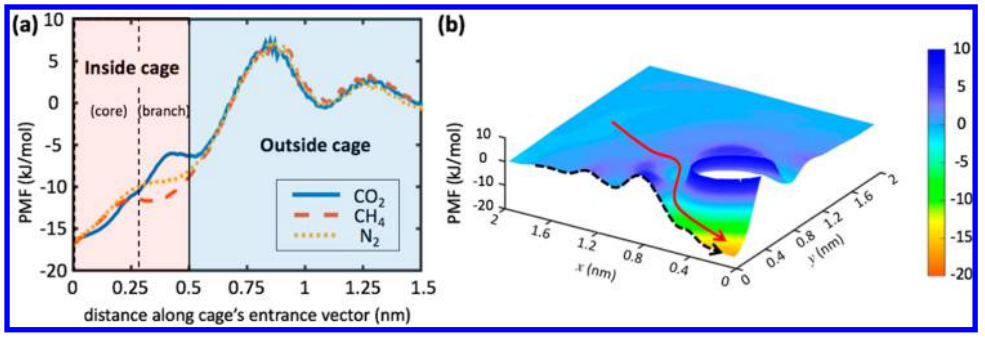

Figure 6. PMF of gas molecules inside and near a cage molecule. (a) One-dimensional PMF along the cage's entrance vector defined in Figure 1b. (b) Two-dimensional PMF for the CO_2 molecule as a function of the distance along and normal to the cage's entrance vector (x is along the entrance vector, and y is normal to the entrance vector; see Figure 1b). The red line denotes a likely pathway for a CO_2 molecule to enter the cage. The black dashed line denotes the PMF along the cage's entrance vector, which was also shown in (a) (blue line). The PMF in (a) has an error bar of ∼0.2−1.2 kJ/mol, with the largest error occurring at a distance of ∼0.8 nm from the cage center.

DOI: 10.1021/acs.jpcb.6b04784
J. Phys. Chem. B 2016, 120, 7195−7200

Figure 6a shows the PMF of different gas molecules along the cage's entrance vector. When the gas molecule is outside the cage (i.e., located at a distance larger than 0.5 nm from the cage center), the PMFs of the three gases show very little difference. A distinct peak of the PMF exists at a distance of 0.85 nm from the cage center, indicating that an energy barrier exists for the gas molecule entering the cage along its entrance vector. This energy barrier originates from the dense packing of solvent molecules outside the cage's access window, which hinders gas from entering into the cage (Figure S3 in the Supporting Information). Inside the cage, the PMFs show a kink/shoulder in the cage's branch regions. For the long CO_2 molecules, this kink originates largely from the entropic penalty of confining it in the narrow rodlike branch regions. For the shorter N_2 and CH_4 molecules, the shoulder is likely caused by the reduced van der Waals attractions with the cage atoms.

The PMF shown in Figure 6a indicates that gas molecules entering in the cage along the cage's entrance vector must overcome an energy barrier of ~7 kJ/mol. However, there may exist other pathways with weaker or no energy barrier. To delineate these other possible pathways, we calculated the two-dimensional (2D) PMFs for gas molecules as a function of their distance along and normal to the cage's entrance vector (shown as the *x*- and *y*-directions in Figure 1b). It is found that these PMFs are qualitatively similar for all three gases. Hence only the 2D PMF for the CO_2 molecule is shown in Figure 6b. It can be seen that there indeed exists an energy barrier-free pathway (marked using a red line) for CO_2 gas molecules to enter the cage. Overall, the PMFs shown in Figure 6 indicate that, for all gases studied here, gas molecules can enter the cage essentially without an energy barrier. However, for gas molecules to leave the cage, they must overcome an energy penalty. This energy penalty depends on the position of the gas molecules inside the cage and can be up to ~16 kJ/mol for each of the gases considered here.

The modest energy penalty for gas molecules to leave a cage suggests that the cage molecule can indeed trap gas molecules. For applications in gas storage, one often needs to know the time scale that a gas molecule can be trapped inside in a cage. To find this time scale, we computed the occupancy autocorrelation function of gas molecules $C_p(t) = \langle P(0)\,P(t)\rangle$, where the bracket $\langle\cdots\rangle$ denotes the ensemble average. $P(t)$ is defined as 1.0 if the gas molecule inside a cage at $t = 0$ continuously resides in the cage until time t. Figure 7 shows that, for all gases, $C(t)$ decays to ~0.1 within ~1 ns. Hence, the mean residence time of a gas molecule inside a cage is on the order of nanoseconds, which suggests that the exchange of the gas molecules inside and outside of the cage is rather rapid.

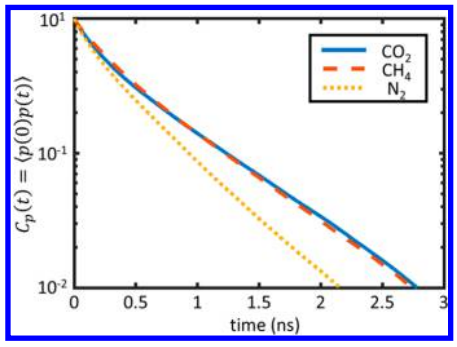

Figure 7. Cage occupancy autocorrelation function for three different gases.

4. CONCLUSIONS

In summary, we have studied the storage of three different gas molecules in a class of porous liquids (crown-ether-substituted cage molecules in a 15-crown-5 solvent) using MD simulations. We have found that the capacity of gas storage in a cage molecule is governed by the nonelectrostatic (dispersive) intermolecular interactions between the gas and the cage and the size/shape of the gas molecules. The former controls the affinity of gas molecules to the cage; the latter mainly controls whether the space inside the cage can be utilized effectively (e.g., whether one can store, simultaneously, one gas molecule in the cage's core and a few others in the cage's branch regions). Due to the competition between these two factors, the cage's gas storage capacity does not correlate simply with the gas molecule's size. All gas molecules studied here can enter the cage without a noticeable energy barrier. However, gas molecules inside a cage must overcome a modest energy penalty before leaving the cage. Despite this, gas molecules inside the cage can exchange rather rapidly with those in the bulk solvents.

The insight gained here on the gas storage in organic cages, along with the knowledge on solubility of gas in the solvents, may help formulate rational design rules for porous liquids for specific applications. For example, for applications targeting N_2/CO_2 separation, our results suggest that increasing the size of the cage molecule's core is desirable. Because the storage of CO_2 molecules inside a cage is limited mainly by the difficulty in packing multiple CO_2 molecules into the cage's core but the storage of N_2 is limited mainly by the weak N_2-cage interactions, this modification of the cage should enhance the storage capacity for CO_2 molecules more greatly than that for the N_2 molecules.

■ ASSOCIATED CONTENT

Ⓢ Supporting Information

The Supporting Information is available free of charge on the ACS Publications website at DOI: 10.1021/acs.jpcb.6b04784.

Discussion of the structural fluctuations of the cage molecules in the porous liquids, the diffusion of solvent molecules in the porous liquids, and the density distribution of solvent molecules along the cage's entrance vector (PDF)

■ AUTHOR INFORMATION

Corresponding Author

*R. Qiao. Phone: 540-231-7199. E-mail: ruiqiao@vt.edu.

Notes

The authors declare no competing financial interest.

■ ACKNOWLEDGMENTS

We thank the ARC at Virginia Tech for generous allocations of computer time on the NewRiver cluster. R.Q. was partially supported by an appointment to the HERE program for faculty at the Oak Ridge National Laboratory administered by ORISE. J.H. acknowledges work performed at the Center for Nanophase Materials Sciences, a US DOE Office of Science User Facility. B.G.S. acknowledges support from the Center for Understanding and Control of Acid Gas-Induced Evolution of Materials for Energy (UNCAGE-ME), an Energy Frontier

DOI: 10.1021/acs.jpcb.6b04784
J. Phys. Chem. B 2016, 120, 7195−7200

Research Center funded by the U.S. Department of Energy (DOE), Office of Science, Basic Energy Sciences.

REFERENCES

(1) Szostak, R. *Molecular Sieves*; Springer: New York, 1989.
(2) Zhou, H. C.; Long, J. R.; Yaghi, O. M. Introduction to Metal-Organic Frameworks. *Chem. Rev.* **2012**, *112*, 673−674.
(3) Simon, P.; Gogotsi, Y. Materials for Electrochemical Capacitors. *Nat. Mater.* **2008**, *7*, 845−854.
(4) Wright, P. A. *Microporous Framework Solids*; Royal Society of Chemistry: Cambridge, U.K., 2008.
(5) Li, H.; Eddaoudi, M.; O'Keeffe, M.; Yaghi, O. M. Design and Synthesis of an Exceptionally Stable and Highly Porous Metal-organic Framework. *Nature* **1999**, *402*, 276−279.
(6) Tozawa, T.; Jones, J. T. A.; Swamy, S. I.; Jiang, S.; Adams, D. J.; Shakespeare, S.; Clowes, R.; Bradshaw, D.; Hasell, T.; Chong, S. Y.; et al. Porous Organic Cages. *Nat. Mater.* **2009**, *8*, 973−978.
(7) Hasell, T.; Zhang, H. F.; Cooper, A. I. Solution-Processable Molecular Cage Micropores for Hierarchically Porous Materials. *Adv. Mater.* **2012**, *24*, 5732−5737.
(8) Brutschy, M.; Schneider, M. W.; Mastalerz, M.; Waldvogel, S. R. Porous Organic Cage Compounds as Highly Potent Affinity Materials for Sensing by Quartz Crystal Microbalances. *Adv. Mater.* **2012**, *24*, 6049−6052.
(9) O'Reilly, N.; Giri, N.; James, S. L. Porous Liquids. *Chem. - Eur. J.* **2007**, *13*, 3020−3025.
(10) Giri, N.; Davidson, C. E.; Melaugh, G.; Del Popolo, M. G.; Jones, J. T. A.; Hasell, T.; Cooper, A. I.; Horton, P. N.; Hursthouse, M. B.; James, S. L. Alkylated Organic Cages: from Porous Crystals to Neat Liquids. *Chem. Sci.* **2012**, *3*, 2153−2157.
(11) Mastalerz, M. Liquefied Molecular Holes. *Nature* **2015**, *527*, 174−176.
(12) Giri, N.; Del Popolo, M. G.; Melaugh, G.; Greenaway, R. L.; Ratzke, K.; Koschine, T.; Pison, L.; Gomes, M. F. C.; Cooper, A. I.; James, S. L. Liquids with Permanent Porosity. *Nature* **2015**, *527*, 216−221.
(13) Jorgensen, W. L.; Maxwell, D. S.; TiradoRives, J. Development and Testing of the OPLS All-atom Force Field on Conformational Energetics and Properties of Organic Liquids. *J. Am. Chem. Soc.* **1996**, *118*, 11225−11236.
(14) Harris, J. G.; Yung, K. H. Carbon Dioxides Liquid-Vapor Coexistence Curve and Critical Properties as Predicted by a Simple Molecular-Model. *J. Phys. Chem.* **1995**, *99*, 12021−12024.
(15) Potoff, J. J.; Siepmann, J. I. Vapor-liquid Equilibria of Mixtures Containing Alkanes, Carbon Dioxide, and Nitrogen. *AIChE J.* **2001**, *47*, 1676−1682.
(16) Liu, B.; Smit, B. Comparative Molecular Simulation Study of CO_2/N_2 and CH_4/N_2 Separation in Zeolites and Metal-Organic Frameworks. *Langmuir* **2009**, *25*, 5918−5926.
(17) Hess, B.; Kutzner, C.; van der Spoel, D.; Lindahl, E. GROMACS 4: Algorithms for Highly Efficient, Load-Balanced, and Scalable Molecular Simulation. *J. Chem. Theory Comput.* **2008**, *4*, 435−447.
(18) Hess, B.; Bekker, H.; Berendsen, H. J. C.; Fraaije, J. G. E. M. LINCS: A Linear Constraint Solver for Molecular Simulations. *J. Comput. Chem.* **1997**, *18*, 1463−1472.
(19) Martinez, L.; Andrade, R.; Birgin, E. G.; Martinez, J. M. PACKMOL: A Package for Building Initial Configurations for Molecular Dynamics Simulations. *J. Comput. Chem.* **2009**, *30*, 2157−2164.
(20) Goursot, A.; Papai, I.; Vasilyev, V.; Fajula, F., Modeling of Adsorption Properties of Zeolites. In *Zeolites: A Refined Tool for Designing Catalytic Sites*; Bonneviot, L.; Kaliaguine, S., Eds.; Elsevier Science: Québec, Canada, 1995; pp 109−116.

DOI: 10.1021/acs.jpcb.6b04784
J. Phys. Chem. B 2016, 120, 7195−7200